Mathematical modeling and simulation of porosity on thermomechanical properties of UHTCs under hypersonic conditions

Zuccarini, C., Ramachandran, K., Russo, S., Jayakody, Y. C. & Jayaseelan, D. D

DOI 10.1002/ces2.10168
ISSN 2578-3270

Publisher: Wiley Open Access

Received: 7 October 2022 | Revised: 25 October 2022 | Accepted: 31 October 2022

DOI: 10.1002/ces2.10168

International Journal of Ceramic Engineering & Science

RESEARCH ARTICLE

Mathematical modeling and simulation of porosity on thermomechanical properties of UHTCs under hypersonic conditions

Carmine Zuccarini[1] | **Karthikeyan Ramachandran**[1] | **Stefano Russo**[2,3] | **Yasith C. Jayakody**[1] | **Doni Daniel Jayaseelan**[1]

[1]Department of Aerospace and Aircraft Engineering, Kingston University, Roehampton Vale Campus, London, UK(Email: k1546465@kingston.ac.uk; K1825123@kingston.ac.uk)

[2]School of Engineering and Materials Science, Queen Mary University of London, London, UK

[3]School of Aerospace, Transport and Materials, Cranfield University, Cranfield, United Kingdom

Correspondence
Doni Daniel Jayaseelan, Department of Aerospace and Aircraft Engineering, Kingston University, Roehampton Vale Campus, Friars Avenue, Wimbledon, London SW15 3DW, UK.
Email: d.daniel@kingston.ac.uk

Abstract

Ultrahigh temperature ceramics (UHTCs) were analyzed for their suitability in hypersonic flight conditions using balanced heat equations, transport equation, and finite element modeling technique. Mathematical model was derived on the assumption that the induced porosity follows linear and parabolic solutions of Laplace equation and applied external load mimicking hypersonic conditions with critical heat flux ranging between 7 and 44 MW/m^2. Simulations were carried out with four different UHTCs combinations and the results outlined a temperature rise exceeding 4700°C with deformation observed on the fixed area and where the heat flux was generated. The influence of porosity had a greater impact on the performance of the material as it led to a reduction in deformation compared to dense samples. Porous UHTCs exhibited a good thermal shock resistance owing to the release of thermal stresses through pores, which also enhanced the thermal insulation of the structure.

KEYWORDS

finite element analysis, heat flux, hypersonic conditions, mathematical modeling, porosity, thermal stress, UHTCs

1 | INTRODUCTION

When a vehicle reaches hypersonic regime (i.e., Mach > 5), substantial aerodynamic heating and thermochemical reactions are observed.[1] Aerodynamic heating causes a temperature rise which can reach thousands of degrees Celsius which often causes shockwave interactions and molecular dissociation.[2] This leads to requirement of materials that should have high-temperature capability with high thermal conductivity. Current state of the art in the field is based upon the principle of ablation, meaning that the thermal protection part is usually made up of carbon reinforced composites that are used as a sacrificial side to dissipate the energy, making the any type of thermal barrier coating or protection systems not reusable and therefore not efficient or commercially viable.[3]

Ultrahigh temperature ceramics (UHTCs) are a class of materials with melting points exceeding 3000°C which could be utilized for applications such as thermal

protection systems and refractory applications.[4,5] The superiority of diborides compared to carbides in thermal conductivity makes them candidate materials for the thermal protection systems in hypersonic applications.[6,7] However, the diborides of Zr and Hf suggested that their insufficient thermal shock and oxidation resistance at high temperature pose a threat which could lead to material failure.[8,9] Thus, recent research has focused on improving the oxidation resistance of UHTCs by incorporating different high oxidation resistance materials into composites structures.[10–12] It has been well documented that the incorporation of SiC up to 30 vol.% into UHTCs not only improved its densification and mechanical behavior but also led to the formation of protective silicate coating on the surface top in an oxidizing environment.[13,14] However, owing to thin borosilicate layer formation at high temperatures in hypersonic regime, this thin coating melts hence exposes the substrate to high temperature (>1600°C) which permits continuous oxidation. Jayaseelan et al. reported that the reinforcement of UHTCs with rare-earth materials could promote in situ formation of oxidation resistant refractory coatings which could prevent further melting.[4,15]

Previously we reported on incorporating porosity onto the UHTCs releases thermal stress enhancing its heat temperature capabilities.[4] Though this could widen up the research on UHTCs in hypersonic conditions, limited studies are available on the effect of induced porosity. Hence, this paper aims to determine the suitability of four different UHTCs at different levels of porosity for its utilization in the hypersonic flight conditions with aid from the finite element analysis. A mathematical model has been created through Laplace equation to induce the porosity model and compared with finite element analysis (FEA) models.

2 | MATHEMATICAL MODELING—SHEAR STRESS FACTOR

Porosity (Θ) of a material is a scalar quantity and is defined as the ratio between volumes of voids (pores) over total volume.[16] Pores in composites could be formed by fluid interactions, where substance with different viscosities interacts with the material for a prolonged period at non constant temperature or through cavitation where changes in temperature and pressure are rapid and intense causing pockets of vacuum in the surrounding environment that generates pores. Pores significantly influence the mechanical properties, material durability, and insulation capacity. Therefore, it is extremely important to see whether porosity can be predicted in advance, given the specific environmental constraints, porosity has also an effect on how fast a shock wave can pass through the materials as well as the overall electric conductivity. Porosity can be defined by a rate of volumes as unitless quantity given by

$$\Theta = \frac{V_f}{V_\Theta} \tag{1}$$

From Du Plessis definition of porosity provided in Equation (1), V_f represents volume of the material at full density, and V_Θ represents the volume of the sample minus the volume of the pores. Three governing conditions were considered an assumption to develop a mathematical equation that could study the effect of porosity on the material properties such as strength, toughness, and Young's modulus. Hence:

1. Conservation of mass
2. Conservation of linear momentum for both flow induced and cavitation
3. Heat distribution to follow Fick's Law of diffusion

Conservation of mass states that the divergence of the velocity field is naught:

$$\nabla \cdot u = 0 \tag{2}$$

which is also known as continuity equation. The second assumption is that flow induced porosity follows the law of conservation of momentum. The transport of fluid momentum within V_Θ is described by the following relationship:

$$\rho \frac{\partial u}{\partial t} + \rho \cdot (u \cdot \nabla) \cdot u + \nabla p - \rho g - \mu \nabla^2 u = 0 \tag{3}$$

where ρ—fluid density, u—flow velocity field, p—pressure, and μ—viscosity. Given the challenges faced to describe flow in each pore section that occurs, the average procedure is introduced where all the parameters of Equation (3) are volumetrically averaged over the fluid part V_f and V_Θ and multiplied by the porosity Θ. Assuming that continuity and transport principles are met, the final assumption is that the change in the rate of temperature is not affected by the change in material density. Therefore, from Fick's law of diffusion

$$\frac{\partial T}{\partial t} + D \frac{\partial^2 T}{\partial x} = 0 \tag{4}$$

where T is the temperature of the material and D represents the diffusion coefficient which is a dependent of material's property. Solving Equation (4) using a separation of variable generates a series of equation that describe

temperature as a function of position and time. The specific discharge q denotes the average volume of the fluid velocity within the pores, and it is used as a dependent variable for nth average equations. Such quantity is equivalent of the expected value of the velocity field in a vacuum by the Du Plessis method, hence,

$$q = \langle u \rangle \tag{5}$$

Equation (5) would yield to

$$\frac{1}{V_f}\int\int\int_{V_\Theta}^{-} u\, du = \frac{\Theta}{V_f}\int\int\int_{V_\Theta}^{-} u\, du \tag{6}$$

Solving the above volume integrals in a three-dimensional vector field would generate functions that describe the induced force responsible (F) for pores also known as shear stress force as a function of porosity, tortuosity (λ), viscosity (μ), density (ρ), velocity, and geometry of the material. However, using the Du Plessis and Masliyah method,[17] this can be defined as

$$F = \frac{42.69}{d^2} \cdot \frac{1-\lambda}{\Theta\lambda^2}\sqrt{1+\left(\frac{\rho u d}{\mu}\right)\cdot\left(\frac{0.117\,\lambda}{1-\lambda}\right)} \tag{7}$$

Considering the diameter of the cylindrical sample to be the characteristic length (d), the diameters of the pores can be estimated by the equation of Du Plessis[18,19]:

$$d_p = \frac{(3\lambda-1)\,d}{2\lambda} \tag{8}$$

Moreover, tortuosity (λ) is given by

$$\lambda = \frac{3}{4\Theta} + \left(\frac{\sqrt{9-8\Theta}}{2\Theta}\right)\cos\left[\frac{4\pi}{3} + \frac{1}{3}\cos^{-1}\left\{\frac{8\Theta^2 - 36\Theta + 27}{(9-8\Theta)^{\frac{3}{2}}}\right\}\right] \tag{9}$$

Solving of Equation (7) will determine the shear stress force which is induced by the porosity and could be found as a function of porosity and diameter. If each of the induced pores has constant diameter, and that the maximum loss of volume is equivalent to a porosity of 10%, and porosity is induced by air, at average hypersonic reentry conditions (velocity = 393 m/s, temperature = 2000°C, density = 0.1553 kg/m^3, dynamic viscosity 6.63×10^{-5} kg/(m s)).

Tortuosity (λ) could be

$$\lambda = \frac{3}{4\times 0.1} + \left(\frac{\sqrt{9-8\times 0.1}}{0.2}\right) \times \cos\left[\frac{4\pi}{3} + \frac{1}{3}\cos^{-1}\left\{\frac{8\times 0.1^2 - 36\times 0.1 + 27}{(9-8\times 0.1)^{1.5}}\right\}\right] = 0.34\ (unitless)$$

Hence the porosity induced shear force is as follows:

$$F_{SHEAR} = \frac{42.69}{0.01^2}\cdot\frac{1-0.34}{0.10\times 0.34^2}\sqrt{1+\left(\frac{0.1553\times 393\times 0.01}{\mu}\right)\cdot\left(\frac{0.117\times 0.34}{1-0.34}\right)}$$

$$F_{SHEAR} = 426\,900\times 57.09\sqrt{1+(9109.77)\times 0.009} = 426\,900\times 517.2 = 220.81\times 10^6\ \text{N}$$

Another assumption made in this study is that the sample operates in the gravitational fields in earth atmosphere; hence, the total intensity of the body force is equal to the gravitational force. Given that the density is the ratio of mass per unit volume, the mass of sample can be estimated as

$$m = \rho_m \cdot V \tag{10}$$

Assuming this is only acting under the effect of gravity and that the density of the material ρ_m is the maximum density of zirconium diboride 6090 kg/m^3; hence, mass of the sample is as follows:

$$m = 6090\times 0.005\times 0.005\times \pi\times 0.02 = 9.56\times 10^{-3}\ \text{kg}.$$

The consideration of gravitational force[20] means that we are assuming the sample that operates at hypersonic speed in the lower earth atmosphere. Hence, the attractive mass considered will be the one of the Earth ($5.9722\cdot 10^{24}$ kg), whereas the distance will be assumed to be the maximum height for lower earth atmosphere (80 km) plus the earth radius (6371 km).

Hence,

$$F_{GRAVITATIONAL} = \frac{6.6740\cdot 10^{-11}\cdot 5.9722\cdot 10^{24}\cdot 9.56\cdot 10^{-3}}{\left(\left(80+6371\right)\cdot 10^3\right)^2}$$

$$= \frac{381.37 \cdot 10^{10}}{\left(6451 \cdot 10^{3}\right)^{2}}$$

$$= \frac{381.37 \cdot 10^{10}}{41.61 \cdot 10^{12}}$$

$$= 9.16 \cdot 10^{-2}\ \text{N}$$

$$F_{BODY} = \frac{6.6740 \times 10^{-11} \times 5.9722 \times 10^{24} \times 3.1 \times 10^{-1}}{7 \times 10^{42}}$$

$$= 2.52 \times 10^{4}\ \text{N}$$

The body force in vacuum is inversely proportional to the gravitational force acting on the sample. Therefore, the ratio of shear stress force is given by

$$f = \frac{F_{BODY}}{F_{SHEAR}} = \frac{F_{SHEAR}}{F_{GRAVITATIONAL} + F_{SHEAR}}$$

$$= \frac{220.81 \cdot 10^{6}\ \text{N}}{\left(9.16 \cdot 10^{-2}\right) + \left(220.81 \cdot 10^{6}\right)\ \text{N}} = 0.99$$

A general solution to the heat equation is as follows:

$$T(t,x) = e^{At} \cdot D_n \cdot B \cos Cx \tag{11}$$

Equation (11) describes the rate of change in temperature as a function of position and time where A and B are arbitrary constants that depend upon initial and boundary conditions. Estimating an exact value for the constant is beyond the scope of this study, assuming that the temperature will change randomly to the maximum melting point of the UHTCs. The constants A and C will be set to 1, whereas B was attained from[21] that solves the equations:

$$B \cos x = 0 \tag{12}$$

Given that B must not be zero then:

$$\cos x = 0 \rightarrow x = \frac{\pi}{2} + 2k\pi \tag{13}$$

Moreover, B is therefore:

$$B = \frac{\pi}{2} + 2k\pi \tag{14}$$

and the temperature function would result in:

$$T(t,x) = e^{t} \cdot D_n \cdot \left(\frac{\pi}{2} + 2k\pi\right) \cos x \tag{15}$$

The use of such methodology both in vacuum and within the earth gravitational field can be used to estimate many different effects of porosity. This paper will focus primarily on the Young modulus for UHTCs in porous material which could be described by Kováčik equation where E is the Young modulus of the material at a given porosity Θ. E_0 is the original Young's modulus of the material where there is no loss of density due to porosity and f is the parametric representation of the shear stress force.[22]

$$E = E_0 \left(1 - \frac{\rho}{\rho_\Theta}\right)^{0.99} \tag{16}$$

3 | MATHEMATICAL MODEL—DENSITY-BASED FORMULATION

The developed mathematical model based on the linear and parabolic solutions is translated into static structural and thermal transient analysis, which were part of the Ansys Workbench package. Zirconium diboride (ZrB_2) and hafnium diboride (HfB_2) and 20 vol.% SiC added diborides were used in the computational study. A time dependent FEA was performed considering samples with no porosity and one with 10 vol.% porosity with a consideration of homogeneously distributed pores. The simulations were carried out to determine temperature distribution, sample deformation, thermal and elastic strains, elastic stress distribution, and shear stress distribution. Samples in cylindrical geometry were analyzed at different heat fluxes on the surface and for different lengths of time assuming one-dimensional heat flow. The transition thermal was implemented to simulate thermal conditions such as heat flux, convection, and radiation, whereas the static structural component was utilized to understand the deformation on the composites. As density is related to porosity, it is possible to demonstrate that a relative density of 90% from our experimental study can be related to a porosity fraction of 0.1 in the samples, and the following equation describes the correlation of the density of the porous material ρ' with respect to the porosity θ and the bulk density of the material ρ.

$$\rho' = (1 - \emptyset)\ \rho \tag{17}$$

Rearranging Equation (17) gives the solution to calculate the porosity through density fraction:

$$\emptyset = 1 - \frac{\rho'}{\rho} \tag{18}$$

Thus, a density fraction of 0.9 is related to the porosity fraction of 0.1. The density values of the composites

TABLE 1 Density of porous and fully dense samples attained from Zapato-Solvas et al.[23]

UHTCs samples	Density without porosity (g/cm^3)	Density with 10 vol.% porosity (g/cm^3)
ZrB_2	6.42 ± 0.5	5.878
ZrB_2—SiC20	6.03 ± 0.03	5.127
HfB_2	10.42 ± 0.5	9.378
HfB_2–SiC20	9.03 ± 0.03	8.127

Abbreviation: UHTCs, ultrahigh temperature ceramics.

were obtained from our previously published work and are tabulated in Table 1.[23]

3.1 | Effect of porosity

The promising characteristics of UHTCs in TPS applications require enormous aerodynamic loads applied toward the structure. This implies that in hypersonic regime, TPS needs to withstand both thermal loads as well as aerodynamics loads constantly. Assuming pores are present homogeneously throughout the UHTCs samples in vacuum, the parametric representation of the shear stress factor induced by the flow is one as per previous experiments by Lam et al.[24]. Further, Θ_C can be assumed as initial porosity using Kováčik equation with potential hypothesised porosity of 10% could be considered both isolated pores and interconnected ones.[25] Unfortunately, pore distribution, size, and shape are unknown for the given set of materials, and there is a need to theoretically simplify the analyzed case. This is accomplishable using a more general equation that does not necessitate the unavailable data. Zhu studied the effect of porosity on Young's modulus of zirconium diboride-based UHTCs and specified that the pores are generalized as completely spherical and observed the same through experimental results and devised in the following equation (19).[26]

$$E = E_0 \left(1 - A\emptyset + B\emptyset^2\right) \tag{19}$$

where E—Young's modulus of the porous material, E_0—Young's modulus of the nonporous material, $\emptyset$ is the porosity fraction of the sample (in this case $\emptyset = 0.1$), and A and B are empirical constants having a value of 1.9 and 0.9, respectively.[26] Wang et al. studied the effect of porosity on the thermal properties of samples of yttria-stabilized zirconia, using a molecular dynamics simulation and determined the inverse relation between thermal conductivity and porosity fraction which in this given environment was expected.[27] The thermal conductivity (k) of the material could be evaluated with the help of thermal diffusivity (D), density (ρ), and heat capacity of the material (C_p) as given in the following equation:

$$k = D\rho C_p \tag{20}$$

The change in thermal conductivity with respect to porosity could be explained by recalling Equation (17), and its relation between porous and nonporous material could be represented as follows:

$$\rho' C_p' = (1 - \emptyset)\ \rho C_p \tag{21}$$

where $\rho'$and C_p' are density and specific heat capacity of the porous material, respectively, whereas ρ and C_p represent density and specific heat capacity of the nonporous materials, and $\varnothing$ is the porosity fraction. Rearranging Equation (21) for thermal diffusivity (D) would result in Equation (22) for nonporous material and Equation (23) for porous material.

$$D = \frac{k}{\rho\, C_p} \tag{22}$$

$$D' = \frac{k'}{\rho' C_p'} \tag{23}$$

Substituting the two previous equations into Equation (17) and rearranging will lead to

$$k' = (1 - \emptyset)\ k\ \frac{D'}{D} \tag{24}$$

where k' represents the thermal conductivity of the porous material, $\varnothing$ is the porosity fraction, k is the thermal conductivity of the nonporous material, and $\frac{D'}{D}$ represents the ratio of thermal diffusivity.

3.2 | Effect of temperature

Temperature excursions at which UHTCs are subjected vary depending on the type of application. Silvestroni et al. reported that in hypersonic vehicle surface, temperatures exceed over 2000°C.[28] Therefore, it is necessity to understand how thermal properties change in the temperature range in which these materials operate. However, most of the materials lack information about thermal properties over 2000°C owing to constraints during measurement at such temperatures using dilatometer or any other techniques as well as reduced access toward extreme techniques as well. A second order approximation equation using thermal strain of UHTCs, and thermal expansion coefficient as shown in Equation (25) where T is the final temperature, T_{ref} is initial temperature for calculating

TABLE 2 Thermal conductivity of ultrahigh temperature ceramics (UHTCs) at different temperature intervals attained from our previous studies[29]

Temperature (°C)	ZrB_2	ZrB_2–SiC20	HfB_2	HfB_2–SiC20
25	103 ± 2	91.5 ± 0.4	112 ± 3	82.3 ± 0.3
200	79 ± 0.4	85.1 ± 0.1	98.3 ± 0.2	77.6 ± 0.1
400	73.8 ± 0.1	80.9 ± 0.1	89.1 ± 0.1	73.4 ± 0.2
600	75.1 ± 0.1	78.2 ± 0.3	83.7 ± 0.3	70.1 ± 0.2
900	85.3 ± 0.2	76.0 ± 0.3	77.7 ± 0.2	66.1 ± 0.2
1200	82.3 ± 0.1	73.8 ± 0.1	74.5 ± 0.1	63.8 ± 0.1
1500	73.3 ± 0.3	70.8 ± 0.4	72.5 ± 0.3	61.0 ± 0.3
1700	68.1 ± 0.3	69.2 ± 0.2	72.1 ± 0.1	59.4 ± 0.3
1900	54.0 ± 0.7	68.3 ± 0.7	70.8 ± 0.5	54.9 ± 0.3

thermal strain, and ΔT is change in temperature, and α_1 and α_2 are first order and second order of thermal expansions. The attained thermal conductivity within the temperature range of 25–1900°C is given in Table 2.

$$\frac{L(T) - L(T_{ref})}{L(T_{ref})} = \alpha_2 \, \Delta T^2 + \alpha_1 \Delta T \tag{25}$$

Data shown in Table 2 indicate that the thermal conductivity decreases steadily with increasing temperature, although there are few exceptions in the case of ZrB_2 where there is significant increase between 600 and 900°C followed with steady decreases similar to other UHTCs trend. Density, thermal expansion coefficient, specific heat capacity, and thermal conductivity are major factors governing the thermal stability of UHTCs.[29] Therefore, specific heat should also be given priority along with diffusivity and conductivity. Earlier work[29] on the determining specific heat of UHTCs led to formation of Equations (26) and (27) which were later manipulated through rules of mixture to form Equation (28) where C_p, C_{p1}, C_{p2}, and C_{pn} are the specific heat capacity of the composite material, first, second, and nth material, and x_1, $x_{2,}$ and x_n are rate among the mass of the first, second, and nth material in the composite and the overall mass of the composites:

$$C_{p-ZrB_2} = 593.40 + 0.05025T + 1.267 \times 10^{-5} \, T^2 - 1.329 \times 10^{-9} \, T^3 - \frac{1.631 \times 10^7}{T^2} \tag{26}$$

$$C_{p-HfB_2} = 366.52 + 0.0391T - \frac{1.150 \times 10^7}{T^2} \tag{27}$$

$$C_p = x_1 \, C_{p1} + x_2 C_{p2} + \cdots + x_n C_{pn} \tag{28}$$

These calculated data, that is, density, Young's modulus, thermal conductivity, thermal expansion coefficient, and specific heat capacity, were utilized as the initial values for assigning the engineering data in the Ansys workbench simulations.

4 | COMPUTER-BASED SIMULATION

4.1 | Effect of heat flux

Extreme heat flux of 7, 15, and 44 MW/m^2 for three holding times of 1.4, 5.5, and 7 s was considered in our present study to analyze the effect of porosity on surface temperature and heat flux of the UHTCs samples using FE model. The boundary conditions for the transient thermal and its deformation study were simple with the bottom surface of the model being fixed with heat flux applied on the top surface. The mesh elemental size was set to 1 mm evenly on the surface of the design. The structural and thermal model provided evidence of variation in deformation and temperature implying the effect of porosity. The distributional behavior of porous UHTCs exhibited less deformation compared to dense samples implicating enhanced thermal capabilities. The increase in temperature capabilities of UHTCs is reported in Figure 1 with increase in the heat flux. For fully dense samples at a heat flux of 44 W/m^2, HfB_2–20SiC exhibited highest temperature value of 4664.7°C, whereas HfB_2 without any silicon carbide reinforcement indicated lowest temperature of 4548.5°C. Likewise, the SiC reinforcement in the most of the samples indicated enhancement in temperature in dense form. The enhancement in the temperature with SiC reinforcement could be due to the formation of borosilicate and zircon layers which could not be predicted through mathematically modeling.[12,13,30]

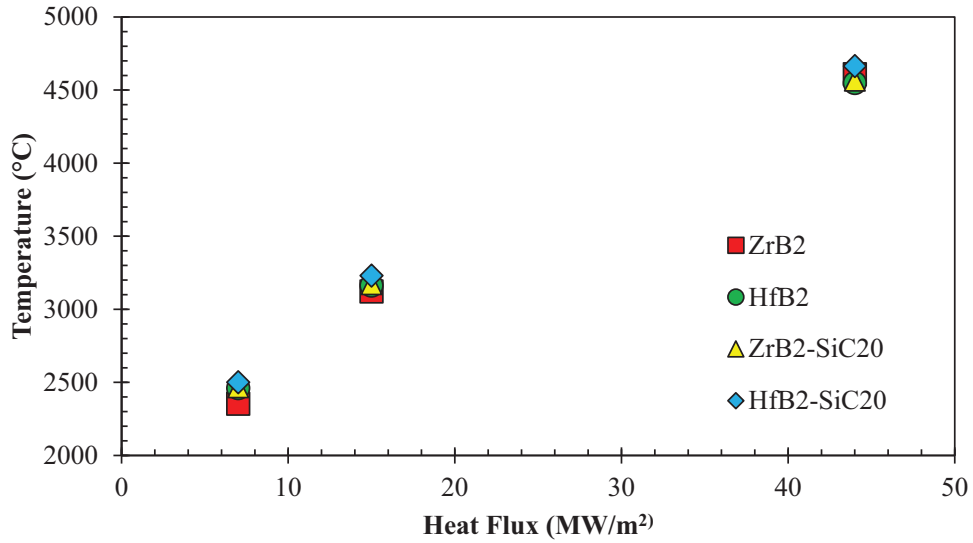

FIGURE 1 Variation of temperature with respect to heat flux of dense ultrahigh temperature ceramics (UHTCs)

TABLE 3 Total deformation of fully dense ultrahigh temperature ceramics (UHTCs) with respect to heat flux

Heat flux (MW/m^2)	Total deformation (in mm)			
	ZrB_2	ZrB_2–SiC20	HfB_2	HfB_2–SiC20
7	0.128	0.119	0.109	0.122
15	0.161	0.104	0.156	0.152
44	0.218	0.201	0.212	0.206

The deformation in fully dense UHTCs is reported in Table 3. From Table 3, it could be inferred that the deformation increases with increase in heat flux. For ZrB_2 with lowest heat flux of 7 W/mm^2, the deformation on the cylindrical sample of dimensions 10 × 10 was about 0.128 mm, whereas with increase in the heat flux upto 44 W/mm^2 resulted in ~50% increase upto 0.218 mm. HfB_2 and UHTCs with SiC reinforcements showcased similar behavior in deformation. The formation of the silicon-based oxide products, while exposed to high temperature on the surfaces, could have reduced the deformation compared to the monolithic ZrB_2 and HfB_2. Although there is reduction on the deformation for the SiC reinforced UHTCs, the structural integrity of the UHTCs modeled was compromised with increase in heat flux. The heat flux applied on the top surface of the cylinder led to deformation on the bottom side of the material forming a draft angle of 0°–2° at the surface as illustrated in Figure 2. This deformation could be due to excess heat flux acting on surface which enhances the thermal stress inside the UHTCs.

On the other hand, the induced porosity model shown enhanced temperature throughout all UHTCs samples along with increase in heat fluxes as plotted in Figure 3. HfB_2–20SiC shown maximum temperature hold of 4787°C for 5 s at heat flux of 44 MW/m^2 comparatively to

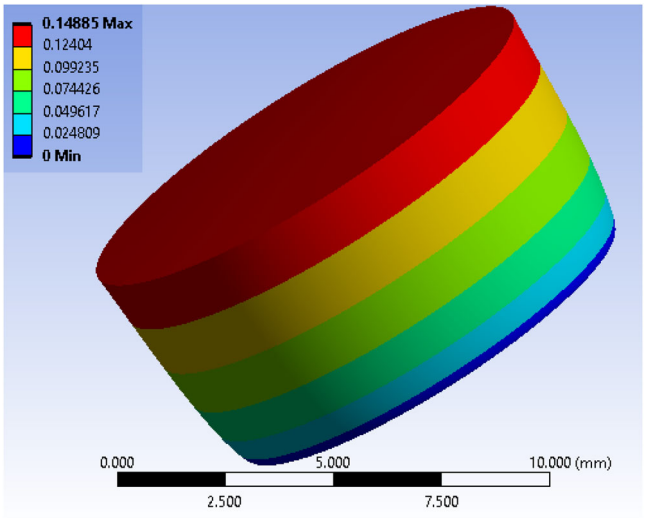

FIGURE 2 Draft angle formation at bottom side of ultrahigh temperature ceramic (UHTC) sample ZrB_2–20SiC at heat flux of 15 MW/m^2 for 5 s

monolithic dense UHTCs. For instance, porous HfB_2 had maximum temperature of 4670.9°C, whereas dense sample had 4548.5°C. Likewise, most of the porous UHTCs had higher surface temperature values compared to its counterparts. This increase of temperature in porous samples over dense could be due to two different reasons (1) the porous nature of composites and (2) fabrication techniques such as spark plasma sintering, hot pressing, and pressureless sintering. In dense sample, heat can be conducted quickly down to entire sample length; hence, the surface temperature drops. However, in porous samples, the pores are good insulators, and hence, it would not conduct away the heat. Hence, the accumulation of heat happens on the

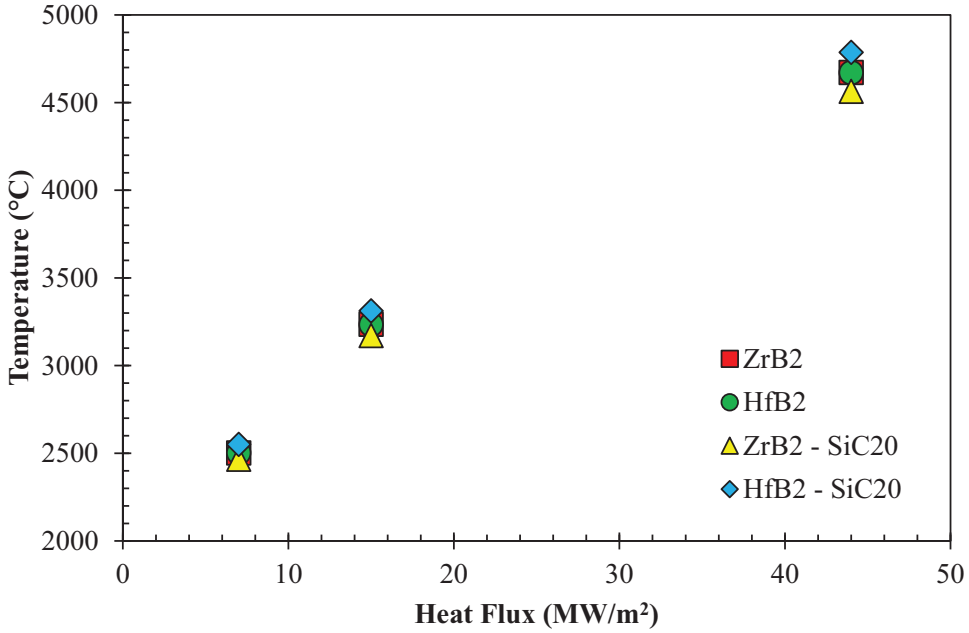

FIGURE 3 Effect of heat flux on porous ultrahigh temperature ceramics (UHTCs) (90% dense) with respect to heat flux

surface, and this is the cause for the increase in surface temperature. Thus, porous nature of the composites helps to release thermal stresses through pores enhancing the thermal shock resistance of the composites. However, due to the presence of pores led to drop in Young's modulus which improved the thermal shock with increase in heat flux.[31] On the other hand, the fabrication technique utilized on UHTCs could also play a huge role. Techniques like spark plasma sintering and hot pressing could enhance the total density of the composite. However, the joule's heating of composites on the surface could lead to the formation of pores, that is, closed (if total porosity ≤10%) and open porosity (if total porosity ≥10%).[32,33] With increase in the joule's heating, the transition from open pores to closed pores enhances the chances of thermal stress loses between the pores leading to higher temperature holdings. Although the effect of the fabrication for pores transition is not evident via FE models, the effect of pores was directly visible from the temperature changes along the samples.

Figure 4 shows the temperature distribution of porous UHTCs at heat flux range of 44 MW/m^2. From Figure 4, maximum temperature region is determined to be at top of surface, and temperature is being distributed throughout the surfaces which was similar to the defocused Nd:YAG laser study by our group earlier.[1] Table 4 reports the structural deformation of the porous UHTCs after the effect of varying heat flux. As reported in Table 4, the deformation in porous samples was reduced compared to the 100% dense samples. For instance, ZrB_2 showcased 0.128 mm displacement in dense state, whereas ZrB_2 with porosity of 10% shown 0.120 mm displacement. Although in the case of the SiC added UHTCs, there was slight increase in the deformation in both HfB_2 and ZrB_2 cases which could have been due to the gas evolution and deterioration at high heat flux testing.

TABLE 4 Total deformation of porous ultrahigh temperature ceramics (UHTCs) under varying heat fluxes

Heat flux (MW/m^2)	Total deformation (in mm)			
	ZrB_2	ZrB_2–SiC20	HfB_2	HfB_2–SiC20
7	0.120	0.119	0.105	0.111
15	0.160	0.158	0.146	0.150
44	0.20	0.216	0.199	0.208

4.2 | Effect of height

Three different heights were studied at varying heat flux to determine the effect of geometry on the UHTCs as represented in Figure 5. The results displayed that the height of the samples had a direct impact on the thermal behavior of the dense as well as porous samples. The dense samples exhibited change in maximum surface temperature of the UHTCs with respect to change in the height/geometry. For instance, HfB_2 for 7 W/mm^2 heat flux showcased maximum surface temperature of 2461°C at height of 5 mm, whereas at 14 and 44 MW/m^2, there was drop of ~7% and ~12% compared to samples at 7 MW/m^2 for the same height of 5 mm. Figure 6 showcases the effect of heat flux of 14 MW/m^2 with respect to change in height for UHTCs samples as shown in Figure 7.

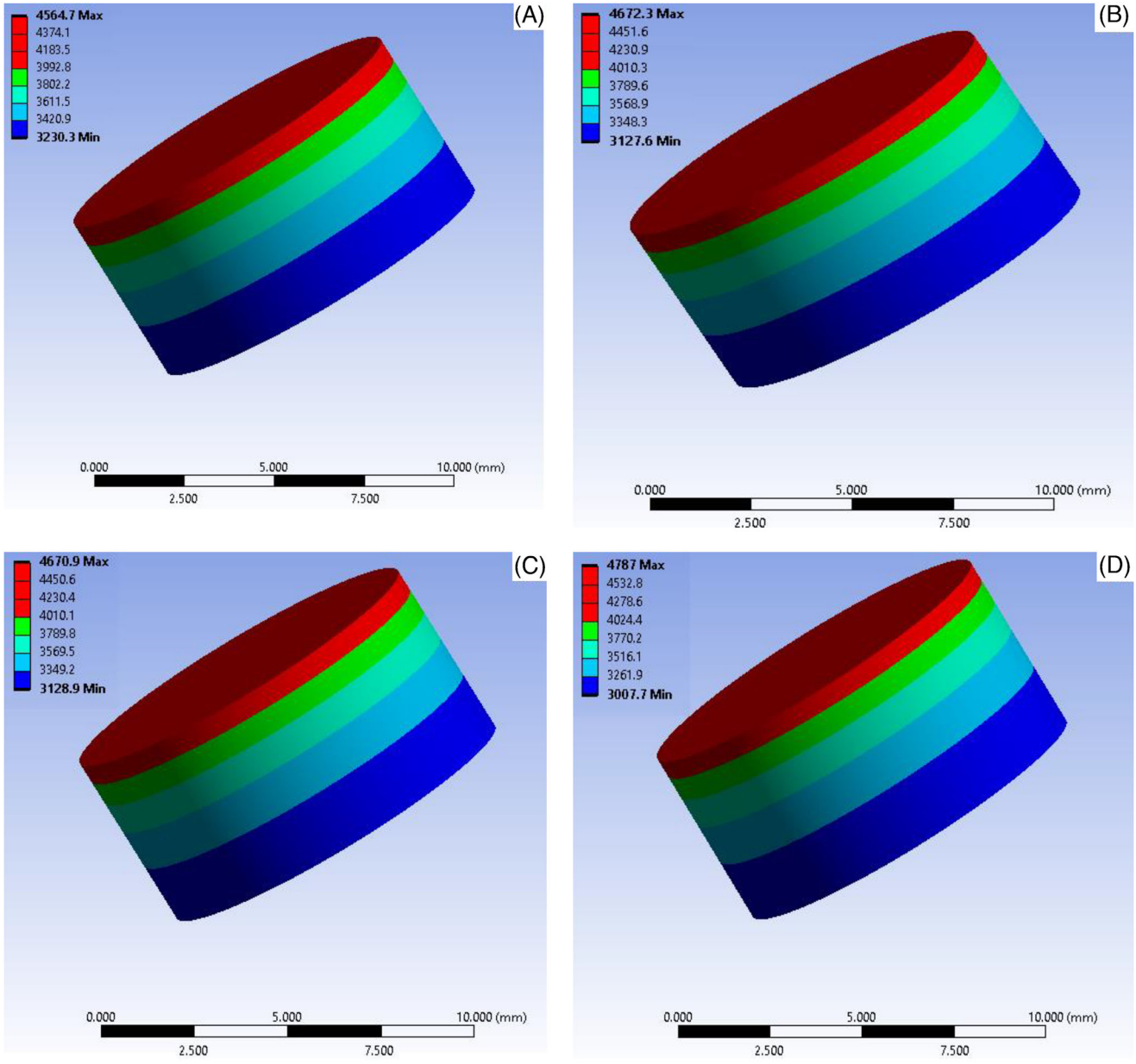

FIGURE 4 Temperature profile of porous ultrahigh temperature ceramics (UHTCs): (A) ZrB_2, (B) ZrB_2–20SiC, (C) HfB_2, and (D) HfB_2–20SiC at 44 MW/m^2

The effect of the height on the samples reduced the maximum surface temperature as it allowed the thermal convection onto the surfaces and leading to enhances spacing for thermal stresses to seep out of the surfaces. On the other hand, the porous UHTCs specimens also showcased same reduction in the temperature like dense UHTCs. However, the surface temperature reductions on the surface of porous UHTCs were comparatively lesser than the dense samples. For instance, the 10% porous HfB_2 for 14 MW/m^2 heat flux indicated a surface temperature of 3159°C for 5 mm height, whereas 2974°C for 20 mm height which was ~6% of the total temperature reduction as illustrated in Figure 8. The 10 mm height HfB_2 sample only indicated a mere loss of ~3 which is less than the dense samples at the same heat flux range. The reduction in the porous samples could be due to the porous gaps present in the samples which release the thermal stresses without affecting the surfaces. This could be supported by the drastic decline on the thermal strain on the UHTCs which enhanced the convection rate of the porous samples. The thermal strains on the dense samples were reduced periodically, whereas in porous samples, there was high reduction on the strain. Porous HfB_2 shown a reduction in thermal strain from 0.175 to 0.165 for height 5–10 mm, whereas dense samples

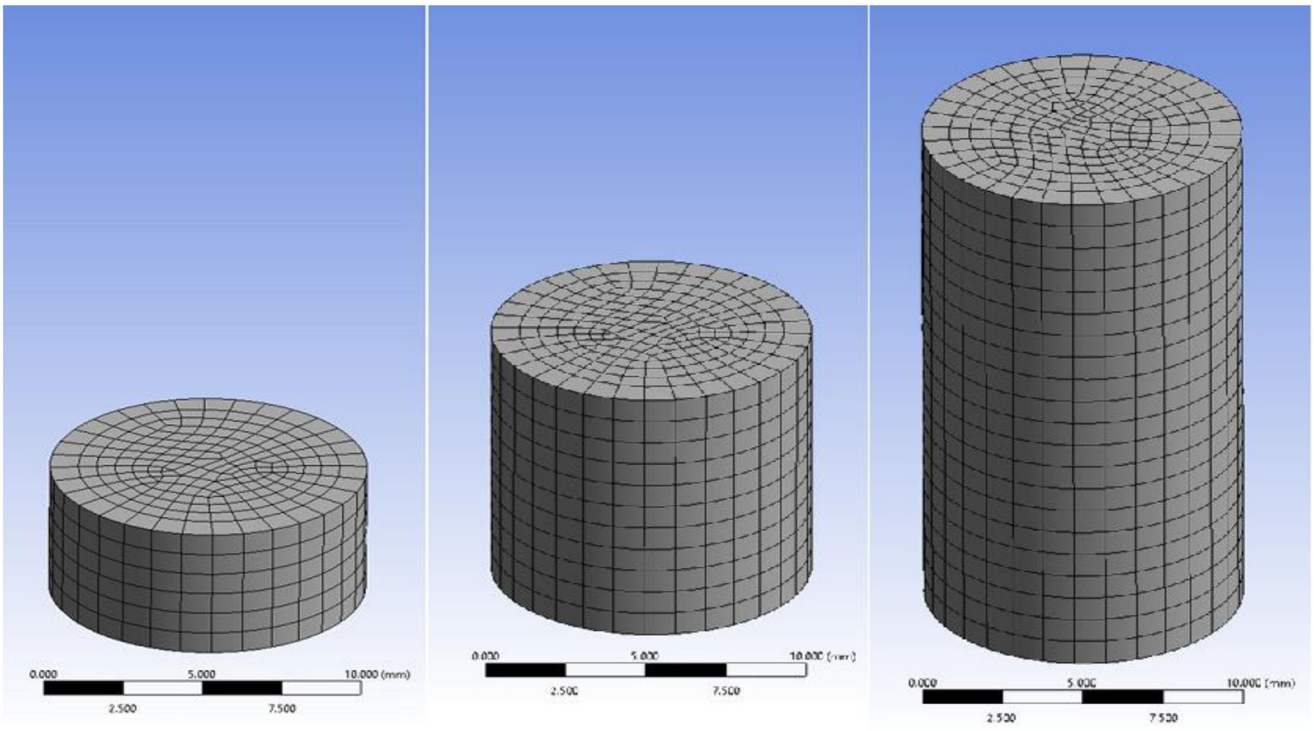

FIGURE 5 Designed geometry and its mesh of the samples from left to right: 10×5, 10×10, and 10×20 mm^2

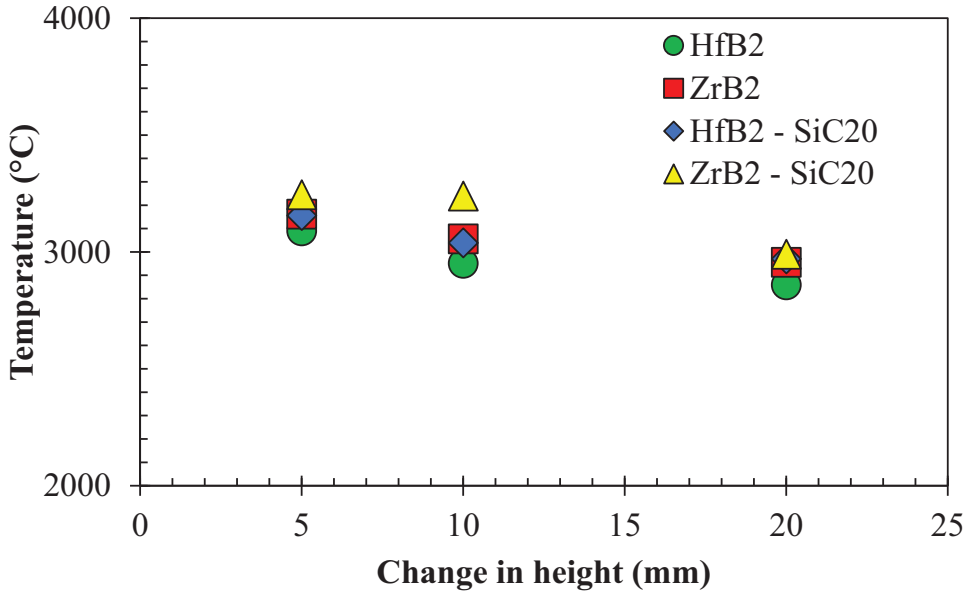

FIGURE 6 Effect of height on the surface temperature of the dense ultrahigh temperature ceramics (UHTCs) samples at 14 MW/m^2

showcased 0.0182–0.0178 mm for same height and heat flux of 7 MW/m^2.

Deformation behaviors of the UHTCs were also seen increasing with increase in heat flux and geometrical changes. This was case for both dense and porous UHTCs. However, increase in geometry of the UHTCs samples enhanced deformation on the surfaces of both dense and porous were closer to one another. The other UHTCs showcased lower total deformation compared to the SiC reinforced HfB_2 at all heat flux regions. Figure 9 showcases the difference in deformation between porous and dense samples of HfB_2–20%SiC at heat flux of

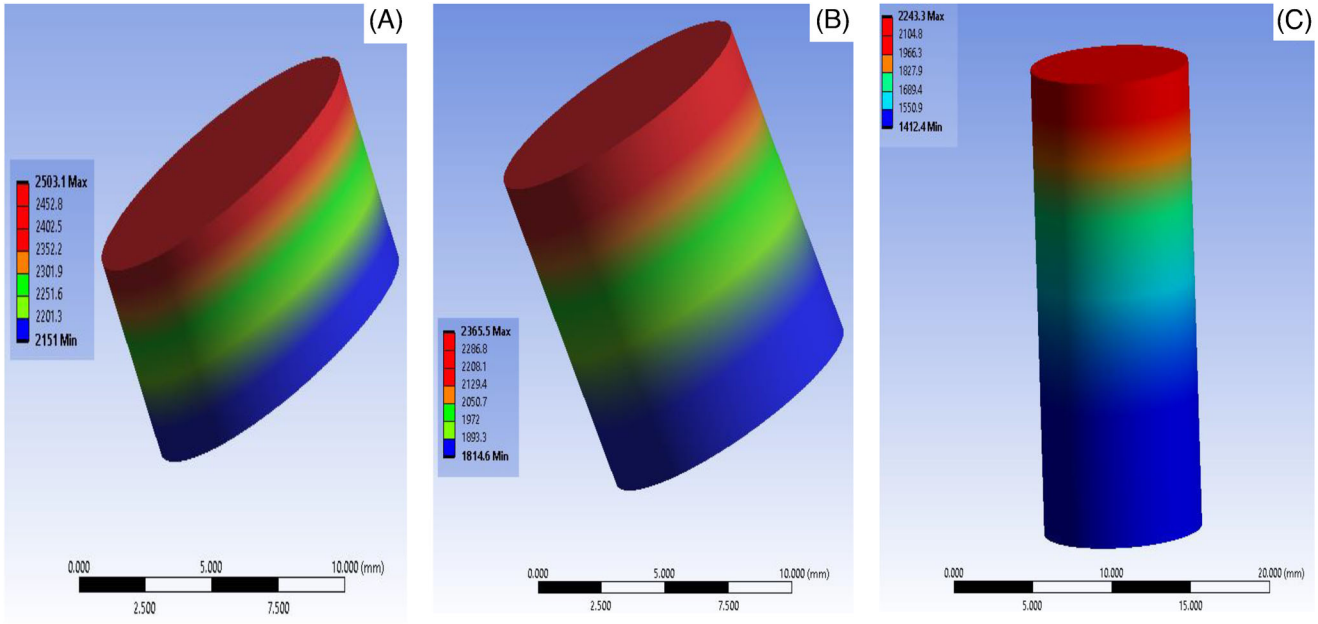

FIGURE 7 Temperature contours of HfB_2 at 7 MW/mm^2

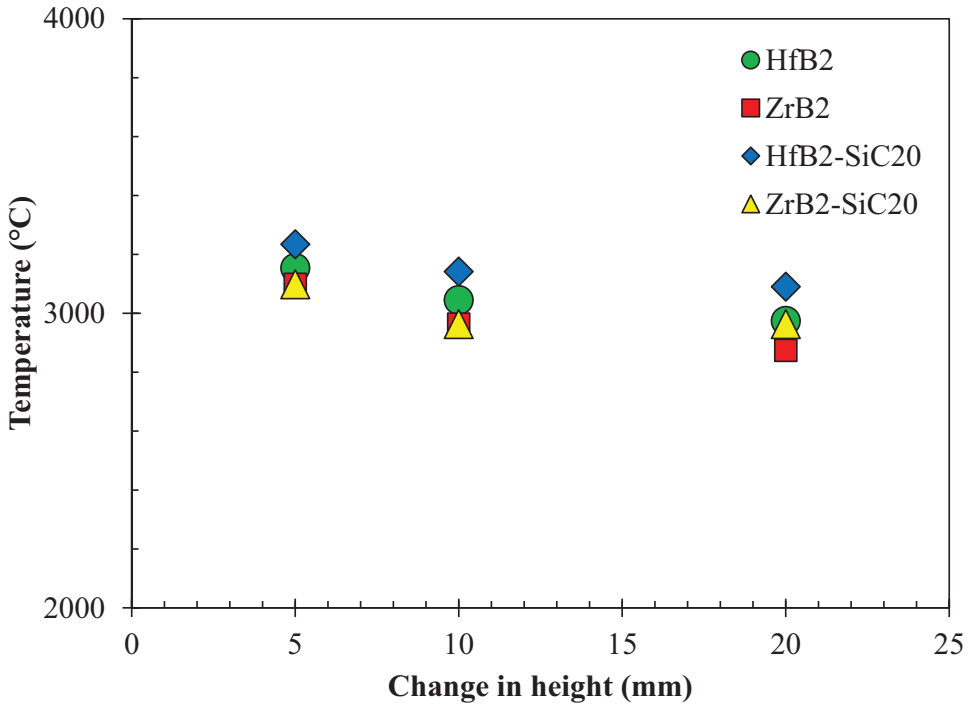

FIGURE 8 Effect of height on the surface temperature of the porous ultrahigh temperature ceramics (UHTCs) samples at 14 MW/m^2

7 MW/m^2. As shown in Figure 8, the porous samples of HfB_2–20%SiC UHTCs have lower deformation at lower heat flux region, whereas with increase in heat flux, the deformation range was closer to one another. This could be due to the release of thermal stress from the pores which did not affect the samples while under heat flux. One more reason could be due to the formation of oxide layers while undergoing higher heat flux which resisted further deformation and oxidation on the surfaces.[1]

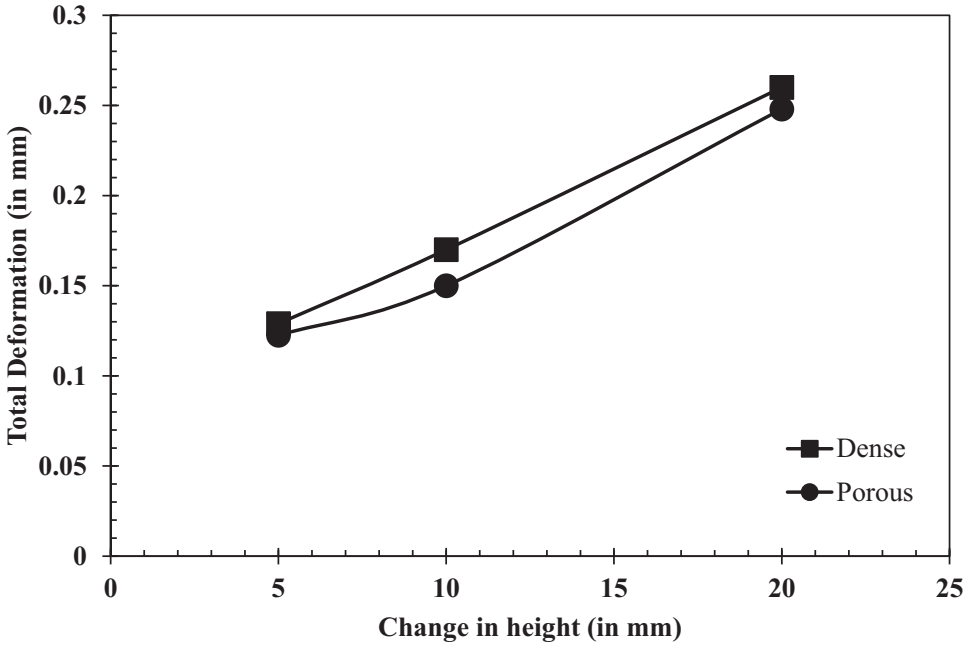

FIGURE 9 Total deformation of HfB_2–20%SiC ultrahigh temperature ceramic (UHTC) in dense and porous forms at heat flux of 7 MW/m^2

5 | CONCLUSION

Diboride-based UHTCs have been a constant field of research for its potential in thermal protection system. Through this paper, mathematical model based on the balanced heat equation, transportation model, and density-based models were designed, and finite element model was proposed to understand the behavior of dense and porous UHTCs such as zirconium diboride, hafnium diboride, and its reinforcement with SiC in UHT condition. The FE model created based on the mathematical calculation showcased that the porous samples exhibited high thermal stability compared to the dense samples. This is attributed to the thermal stresses released from the pores which assists the enhanced thermal capabilities. On the other hand, the reinforcement of SiC led to degradation on UHTCs deformation in both dense and porous samples due to gases evolution. Further, with change in the geometry of the model led to reduction in the maximum surface temperature as it allowed the thermal convection onto the surfaces and leading to enhance spacing for thermal stresses to seep out of the surfaces. The FE model showcased the importance of having porous nature at critical heat fluxes at hypersonic conditions. Although this study was successful in providing evidence of porous behavior of UHTCs, one important limitation of the study was it lacked airflow, that is, the UHTCs were static throughout the study. This limitation led to non-consideration of chemical behavior and fluid structure interaction between materials at high temperatures.

ACKNOWLEDGMENT

Authors C Zuccarini, K Ramachandran, and YC Jayakody would like to acknowledge Kingston University for the support toward their PhD research.

NOMENCLATURE

Symbol	abbreviation
Θ, θ	porosity
V_f	volume of the material at full density
V_Θ	volume of the porous material
V	volume
$\nabla \cdot u$	divergence of velocity in the X direction
ρ, ρ_m	density
ρ'	density of the porous material
∂	partial derivative
t	time
p	pressure
μ	viscosity
T	temperature
D	diffusion coefficient
F, F_{SHEAR}	shear stress force
λ	tortuosity
d	diameter of the cylindrical sample
m	mass
E	Young's modulus
E_0	Young's modulus of nonporous material
k'	thermal conductivity of porous material
k	thermal conductivity of nonporous material
α_1	first order of thermal expansions
α_2	second order of thermal expansions

T_{ref} initial temperature

ORCID

Karthikeyan Ramachandran https://orcid.org/0000-0003-2246-7309
Stefano Russo https://orcid.org/0000-0002-5673-4420
Doni Daniel Jayaseelan https://orcid.org/0000-0002-2489-637X

REFERENCES

1. Paul A, Jayaseelan D, Venugopal S, Zapato-Solvas E, Binner J, Vaidhyanathan B, et al. UHTC composites for hypersonic applications. Am Ceram Soc. 2012;91(1):22–29B.
2. Allen HJ. The aerodynamic heating of atmosphere entry vehicles – a review. Washington: NASA; 1964.
3. Szczepaniak R, Kozun G, Przybylek P, Komeorek A, Krzyzak A, Woroniak G. The effect of the application of a powder additive of a phase change material on the ablative properties of a hybrid composite. Compos Struct. 2021;256(113041):1–13.
4. Zapato-Solvas E, Jayaseelan D, Brown P, Lee W. Thermal properties of La_2O_3-doped ZrB_2- and HfB_2-based ultra-high temperature ceramics. J Eur Ceram Soc. 2013;33(15–16):3467–72.
5. Wuchina E, Opila E, Opeka M, Fahrenholtz B, Talmy I. UHTCs: ultra-high temperature ceramic materials for extreme environment applications. Electrochem Soc Interface. 2007;16(4):30–6.
6. Monteverde F. 35th International Conference and Exposition on Advanced Ceramics and Composites. Daytona Beach: American Ceramic Society; 2011.
7. Ramachandran K, Boopalan V, Bear J, Subramani R. Multi-walled carbon nanotubes (MWCNTs)-reinforced ceramic nanocomposites for aerospace applications: a review. J Mater Sci. 2022;57(2):3923–53.
8. Glaser F, Post B. System zirconium-boron. Trans Metall Soc. 1953;5:1117–8.
9. Jayaseelan D, Pramana S, Grasso S, Bai Y, Skinner S, Reece M, et al. Fabrication and characterisation of single-phase $Hf_2Al_4C_5$ ceramics. J Eur Ceram Soc. 2022;42(4):1292–301.
10. Guo S-Q. Densification of ZrB_2-based composites and their mechanical and physical properties: a review. J Eur Ceram Soc. 2009;29(6):995–1011.
11. Fahrenholtz W, Hilmas G, Talmy I, Zaykoski J. Refractory diborides of zirconium and hafnium. J Am Ceram Soc. 2007;90(5):1347–64.
12. Eakins E, Jayaseelan D, Lee W. Toward oxidation-resistant ZrB_2-SiC ultra high temperature ceramics. Metall Mater Trans A. 2011;42:878–87.
13. Rezaie A, Fahrenholtz W, Hilmas G. Oxidation of zirconium diboride–silicon carbide at 1500°C at a low partial pressure of oxygen. J Am Ceram Soc. 2006;89(10):3240–5.
14. Zuccarini C, Ramachandran K, Jayaseelan DD, Mudiyanselage YCJ. "Stress distribution analysis in zirconium diboride and silica carbide (ZrB_2-SiC) based thermal protection system under hypersonic flight conditions using a machine learning driven approach" in "Ultra-High Temperature Ceramics: Materials For Extreme Environment Applications V", Daniel Butts, MACH-20, LLC, USA; Carmen Carney, Air Force Research Laboratory, USA; Carolina Tallon, Virginia Tech, USA; Gregory Thompson, University of Alabama, USA; Chris Weinberger, Colorado State University, USA Eds, ECI Symposium Series, (2022). https://dc.engconfintl.org/uhtc_v/48
15. Jayaseelan D, EZ-Solvas, PB, Lee W. In situ formation of oxidation resistant refractory coatings on SiC-reinforced ZrB_2 ultra high temperature ceramics. J Am Ceram Soc. 2012;95(4):1247–54.
16. Zivcova Z, Gregorova E, Pabst W, Smith D, Michot A, Poulier C. Thermal conductivity of porous alumina ceramics prepared using starch as a pore-forming agent. J Eur Ceram Soc. 2009;29(3):347–53.
17. Du Plessis JP. Mathematical modelling of flow through porous membranes. Pretoria: Department of Applied Mathematics, University of Stellenbosch; 1993.
18. Bird RB, Stewart WE, Lightfoot EN. Transport phenomena. Hoboken, NJ: Wiley; 2006.
19. Zkauskas A. Heat transfer from tubes in crossflow. Adv Heat Transfer. 1987;18:87–159.
20. Bakry M, Eid A, Khader M. Torsion and shear effect on a Big Rip model in a gravitational field. Astrophys Space Sci. 2021;366:97.
21. Tan S, Jalil M. Introduction to the physics of nanoelectronics. Woodhead Publishing in Materials; 2012. Sawston, Cambridge.
22. Szymkiewicz A. Mathematical models of flow in porous media. In: Modelling water flow in unsaturated porous media. Berlin: Springer; 2012. p. 9–46.
23. Zapato-Solvas E, Jayaseelan D, Lin H, Brown P, Lee W. Mechanical properties of ZrB_2- and HfB_2- based ultra-high temperature ceramics fabricated by spark plasma sintering. J Eur Ceram Soc. 2013;33(7):1373–86.
24. Lam D, Lange F, Evans A. Mechanical properties of partially dense alumina produced from powder compacts. J Am Ceram Soc. 1994;77:2113–7.
25. Kováčik J. Correlation between Young's modulus and porosity in porous materials. J Mater Sci Lett. 1999;18:1007–10.
26. Zhu S. Densification, microstructure, and mechanical properties of zirconium diboride based ultra-high temperature ceramics. Rolla, Missouri: Missouri University of Science and Technology; 2008.
27. Wang X, Liu X, Chen Q, Huang W, Pilla S, Liang G. Understanding the effect of porosity on thermal properties of yttria-stabilized zirconia using molecular dynamics simulation. J Mol Liq. 2016;222:88–93.
28. Silvestroni L, Mungiguerra S, Sciti D, Di Martino GD, Savino R. Effect of hypersonic flow chemical composition on the oxidation behavior of a super-strong UHTC. Corros Sci. 2019;159:108125.
29. Zapato-Solvas E, Jayaseelan D, Vandeperre L, Lee B, Venugopal S, Paul A, et al. Ultrahigh temperature ceramic structures multilayered and hybrid ultra-high temperature ceramics. London, UK: Imperial College London; 2012.
30. Gao D, Zhang Y, Fu J, Xu C, Song Y, Shi X. Oxidation of zirconium diboride–silicon carbide ceramics under an oxygen partial pressure of 200 Pa: formation of zircon. Corros Sci. 2010;52(10):3297–303.
31. Ramachandran K, Leelavinodhan S, Antao C, Copti A, Mauricio C, Jyothi Y, et al. Analysis of failure mechanisms of oxide – oxide ceramic matrix composites. J Eur Ceram Soc. 2022;42(4):1626–34.

32. Arunkumar T, Anand G, Subbiah R, Karthikeyan R, Jeevahan J. Effect of multiwalled carbon nanotubes on improvement of fracture toughness of spark-plasma-sintered yttria-stabilized zirconia nanocomposites. J Mater Eng Perform. 2021;30: 3925–33.
33. Ramachandran K, Subramani R, Arunkumar T, Boopalan V. Mechanical and thermal properties of spark plasma sintered alumina-MWCNTs nanocomposites prepared via improvised colloidal route. Mater Chem Phys. 2021;272: 125034.

How to cite this article: Zuccarini C, Ramachandran K, Russo S, Jayakody YC, Jayaseelan DD. Mathematical modeling and simulation of porosity on thermomechanical properties of UHTCs under hypersonic conditions. Int J Ceramic Eng Sci. 2023;5:e10168. https://doi.org/10.1002/ces2.10168